Breakup threshold anomaly in the near-barrier elastic scattering of ^{6}Li + ^{116,112}Sn

N. N. Deshmukh, S. Mukherjee,* D. Patel, N. L. Singh, and P. K. Rath
Physics Department, Faculty of Science, The M.S. University of Baroda, Vadodara-390002, India

B. K. Nayak, D. C. Biswas, S. Santra, E. T. Mirgule, L. S. Danu, Y. K. Gupta, A. Saxena, and R. K. Choudhury
Nuclear Physics Division, Bhabha Atomic Research Centre, Mumbai-400085, India

R. Kumar
Inter-University Accelerator Centre, Aruna Asaf Ali Marg, New Delhi-110067, India

J. Lubian, C. C. Lopes, E. N. Cardozo, and P. R. S. Gomes
Instituto de Física, Universidade Federal Fluminense, Av. Litoranea s/n, Gragoatá, Niteroi, R.J., 24210-340, Brazil
(Received 12 November 2010; published 16 February 2011)

We have measured the elastic scattering of the weakly bound ^{6}Li on the ^{116,112}Sn targets, at energies close to the Coulomb barrier. The energy dependence of the interaction potential has been investigated by two different methods and the presence of the breakup threshold anomaly is observed. We have also derived the total reaction cross sections for the above systems and compared them to those of other systems with halo, weakly bound, and tightly bound projectiles on targets with similar masses. The reaction cross sections are largest for systems with halo nuclei, then the systems with no-halo weakly bound nuclei, and the smallest cross sections are those for tightly bound systems.

DOI: 10.1103/PhysRevC.83.024607 PACS number(s): 25.70.Bc, 25.70.Mn

I. INTRODUCTION

It is a well-established fact that the near barrier elastic scattering of tightly bound heavy ions display an energy dependence of the interacting optical potential (OP) known as a threshold anomaly (TA) [1–3]. The basic characterization of the above terminology is the observation of a localized peak in the real part of the potential accompanying a sharp decrease of the imaginary part of the potential as the bombarding energy declines toward the Coulomb barrier. The name "anomaly" comes from the expectation that the real and imaginary parts of the OP are energy independent at higher energies, but not at near barrier energies. The TA has been understood in the sense that an attractive polarization potential ΔV arises from the coupling of elastic scattering to the other reaction channels at low energies, leading to a real potential $V_{\rm eff} = V_0 + \Delta V$, where V_0 is the real potential at higher energies. In brief, the coupling to channels other than elastic introduces an attractive real potential, and the result of the decrease of the imaginary potential is tacit by the closure of the nonelastic channels at energies near and below the Coulomb barrier. It has been shown [4,5] that there is a connection between the real and imaginary parts of the OP owing to causality and subsequently they obey the dispersion relation. The attractive polarization potential has the effect of enhancing the fusion cross section, because it decreases the Coulomb barrier.

This situation may change in the scattering of weakly bound nuclei [6]. These nuclei have very low breakup threshold energies and so they have a large breakup (BU) probability. At energies above the barrier, fusion cross sections are usually larger than BU cross sections, but at energies close to the barrier, the opposite occurs, and, furthermore, BU probabilities remain large even at energies below the Coulomb barrier [7–16]. The BU process feeds states in the continuum and produces a repulsive polarization potential [17–25]. This fact is compatible with the recently demonstrated [26–28] systematic suppression of a fusion cross section of weakly bound systems at near barrier energies, owing to the dynamic effects of BU.

Therefore, the net polarization potential in the scattering of weakly bound nuclei has two components: one attractive, owing to the couplings of the elastic channel with inelastic excitations and other direct reactions, and one repulsive, owing to the BU. The relative importance of each component determines the final behavior of the polarization potential: If the attractive potential predominates, the usual TA may still be observed. Otherwise, an "anomalous behavior" will be observed for such systems, where, ironically, the new "anomaly" will be the absence of the TA. In such a situation one may say that the system presents the breakup threshold anomaly (BTA) [29,30]. So, contrary to what is written in some papers in the literature, BTA is the absence of TA at the Coulomb barrier, and not necessarily the rise of the imaginary potential when the bombarding energy decreases toward the barrier. Because the BU cross section does not decrease significantly in the vicinity of the Coulomb barrier, this is no longer the threshold of the closing of the reaction channels. When the repulsive BU polarization predominates, BTA is more clearly observed by an increase of the imaginary potential as the energy decreases, associated with a small reduction in the real part of the potential near the barrier. In any situation, the real and imaginary parts of the OP should satisfy the dispersion relation.

*smukherjee_msuphy@yahoo.co.in

Although there have been several works on the elastic scattering of weakly bound nuclei, both stable [13–15,17, 18,29–48] and radioactive [49–51], a systematic behavior of the energy dependence of the OP for such systems has not yet been reached. One of the reasons is that the net polarization potential, composed by competing attractive and repulsive parts, depends strongly on the properties of the weakly bound projectiles, such as their BU energy threshold and the presence of bound inelastic states. The target structure also plays an important role, because it may produce a strong attractive polarization potential, and the relative importance of the Coulomb BU depends on the target mass. Another reason is concerned with the difficulties of the measurements, because one needs very precise data in a large range of the scattering angle and at low energies, where the scattering is almost entirely of the Rutherford type, and therefore it is difficult to extract the interaction potential from the data. One example of this last difficulty is the fact that, among several works in this field, only very recently [41] was it possible to estimate, from experimental data extrapolation, the energy below the Coulomb barrier for which the imaginary potential vanishes.

In the present work we try to contribute to this field by investigating the elastic scattering of the ^{6}Li $+^{116,112}$ Sn systems through very precise and complete angular distributions at energies from below the Coulomb barrier to approximately twice this value. The ^{6}Li projectile has a BU ($\alpha + d$) threshold energy of 1.48 MeV and no bound excited state. We also derive the total reaction cross sections for these systems and compare them with cross sections for other weakly and tightly bound systems with targets in the same mass region, in order to investigate the role of BU on the total reaction cross section.

In Sec. II we describe the experiments. In Sec. III we analyze the data by using both the Woods-Saxon form and double-folding potentials, and investigate their energy dependence and the presence of the TA or BTA. In Sec. IV we study the systematic behavior of the total reaction cross sections for several systems with targets in the same mass region. Finally, we present the summary and main conclusions.

II. EXPERIMENTAL DETAILS

The experiment was performed at the Bhabha Atomic Research Centre–Tata Institute of Fundamental Research (BARC-TIFR) Pelletron facility, Mumbai, India. The beam of ^{6}Li^{+3} was delivered by the 14UD Pelletron accelerator covering the energy range from below to twice the Coulomb barrier (the nominal barrier is ∼22.4 MeV): 20, 21, 22, 23, 26, 30, and 35 MeV for the ^{6}Li $+^{116}$ Sn system, and 21, 23, 25, and 35 MeV for the ^{6}Li $+^{112}$ Sn system. Beam currents ranged between 2.5 and 30 nA. The beam energies were corrected for the half target thickness in the analysis process, which amounts to a maximum of 92 keV for 20 MeV and a minimum of 63 keV for 35 MeV for the ^{6}Li $+^{116}$ Sn system and a maximum of 110 keV for 21 MeV and a minimum of 79 keV for 35 MeV for the ^{6}Li $+^{112}$ Sn system. The beam bombarded consecutively the 450 and 540 μg/cm^2, self-supported enriched ^{116,112}Sn ($\geqslant$98% and 99.5%) targets, respectively, and the elastically scattered ^{6}Li ions were detected by three solid-state silicon

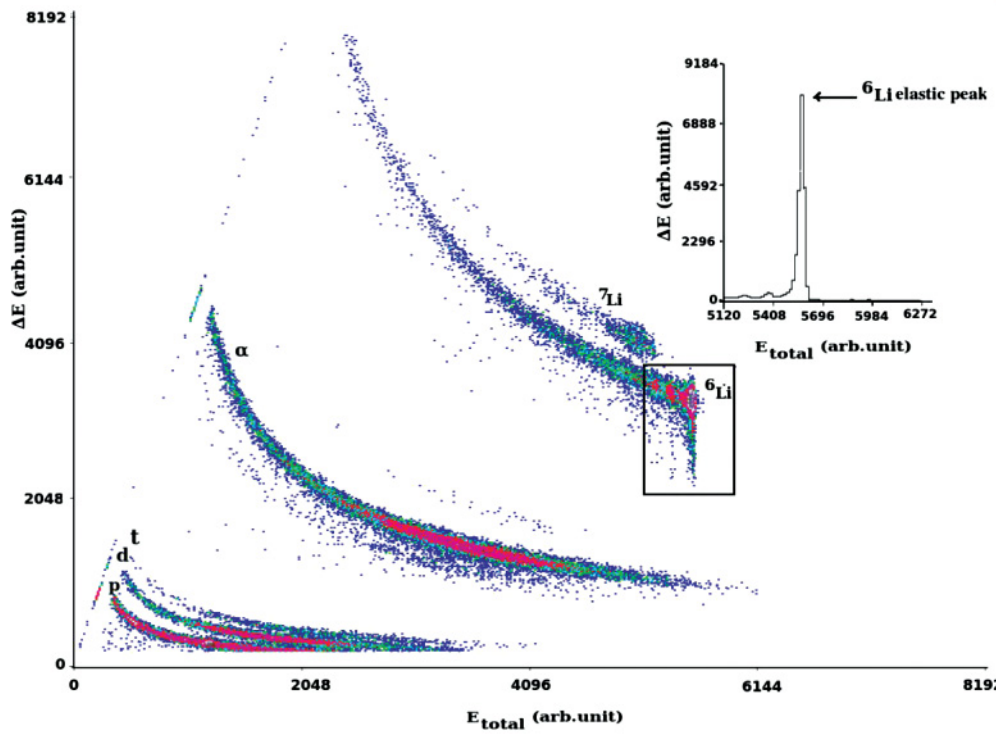

FIG. 1. (Color online) A typical biparametric E-ΔE spectrum for the ^{6}Li+^{116}Sn system at $E_{\rm Lab} = 35$ MeV and $\theta = 35^{\circ}$. The projection of the ^{6}Li elastic peak of the biparametric E-ΔE spectrum is shown in the inset.

surface barrier detectors in $\Delta E + E$ telescopic arrangements. The telescopes used had a thickness (T_1) with $\Delta E = 30$ μm and $E = 300$ μm, (T_2) with $\Delta E = 25$ μm and $E = 1$ mm, and (T_3) with $\Delta E = 50$ μm and $E = 2$ mm. Two monitor detectors with thicknesses $M_1 = 200$ μm and $M_2 = 600$ μm were used for absolute normalization and beam monitoring. The telescopes were placed on a rotating arm inside a 1-m scattering chamber at an angular separation of 10° between consecutive telescopes, and the monitors were placed at ±20°. The angular distributions were measured in steps of 2.5°–5° at angles from 20° to 173° at lower energies and from 20° to 105° for higher energies. The measured statistical error in the data was less than 1% in the forward angles and a maximum of 2% at the backward angles. Figure 1(a) shows a typical biparametric $E - \Delta E$ spectrum for the ^{6}Li+^{116}Sn system at $E_{\rm Lab} = 35$ MeV and $\theta = 35°$. The inset of Fig. 1 shows the corresponding projection for the $Z = 3$ events.

III. OPTICAL MODEL ANALYSIS OF ELASTIC SCATTERING

In this section we present the analysis of the elastic scattering angular distribution data. We use two different kinds of potential in order to check the consistency of the results that should be model independent. In Sec. III A we describe the analysis with a phenomenological Woods-Saxon form interaction potential, and in Sec. III B the analysis is performed by using the double-folding São Paulo potential (SPP) [52,53].

A. Analysis using the phenomenological Woods-Saxon potential

The optical model fits to the elastic scattering data were performed using the ECIS code [54]. We used the real and volumetric imaginary potentials of the Woods-Saxon form. In order to avoid a fit procedure with too many parameters, we started the fit by changing only the real and imaginary depths of the potential, keeping the real and imaginary reduced radii and diffuseness as 1.06 and 0.67 fm, respectively. After this first fit was done, once more we kept the radii fixed and we fitted the depths of the real and imaginary potentials, but this time we varied the diffuseness from 0.49 to 0.57 fm, in steps of 0.02 fm. For the lowest energy it was necessary to reduce the diffuseness of the potentials to 0.43 fm to obtain physical values (attractive real nuclear potential and absorption of flux). Very good fits to the data were obtained but, as usual, we found several families of optical potential parameters that describe the angular distributions equally well. To reduce the ambiguities, we determined the radii of sensitivity R_{Sr} and R_{Si}, corresponding to the real and imaginary radii, where different potentials have the same value. The derived mean sensitivity radii were 10.28 and 8.52 fm, respectively. Figures 2(a) and 2(b) show families of potentials that give similar fits, and the derivation of the real and imaginary sensitivity radii, respectively, for 35 MeV. With an average sensitive radius $R_{Sr} = 9.40$ fm (average between R_{Sr} and R_{Si}) and a mean diffuseness $a = 0.53$ fm for highest energies and $a = 0.43$ fm for lowest energy, we calculated the energy dependence of the

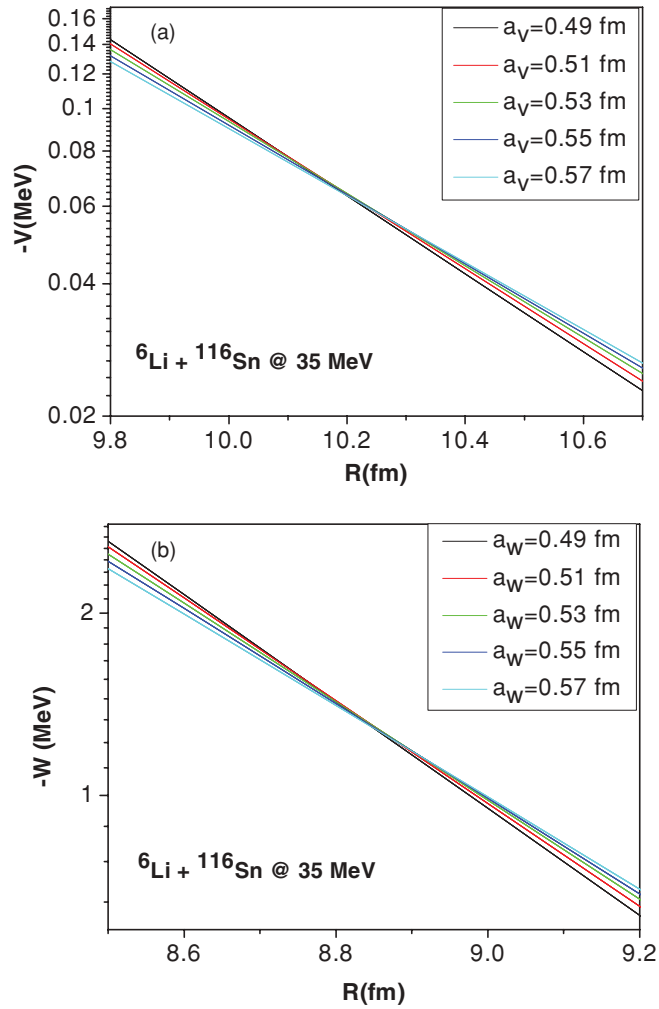

FIG. 2. (Color online) Several potentials that produce similar fits of the data, for 35 MeV. The crossing points are the derived real (a) and imaginary (b) sensitivity radii.

real and imaginary potentials at this radius. For the ^{6}Li+^{112}Sn system the mean diffuseness was kept at $a = 0.67$ fm so as to derive the total reaction cross sections. The values of r_v and r_i were kept at a fixed value of 8.37 fm each in the entire calculation. Table I shows the potential parameters that best fit the data for the ^{6}Li+^{116}Sn system, whereas Table II shows the same for the ^{6}Li+^{112}Sn system. Figures 3 and 4 show the experimental elastic scattering angular distributions and the

TABLE I. Parameters used with Wood-Saxon potential calculations for the ^{6}Li+^{116}Sn system.

$E_{\rm Lab}$ (MeV)	a_r and a_i (fm)	V_r (MeV)	V_i (MeV)	χ^2/n	σ_R (mb)
20	0.43	222.7	2230	11.4	274
21	0.53	89	168	3.7	329
22	0.53	101	244.5	7.6	521
23	0.53	95	100	5.3	555
26	0.53	157	163	35.3	1037
30	0.53	95	68	8.7	1261
35	0.53	148	236	13.6	1826

TABLE II. Parameters used with Wood-Saxon potential calculations for the ^{6}Li+^{112}Sn system.

$E_{\rm Lab}$ (MeV)	a_r and a_i (fm)	V_r (MeV)	V_i (MeV)	χ^2/n	σ_R (mb)
21	0.67	17	25	5.00	235
23	0.67	16	24.7	5.33	480
25	0.67	18	26	4.92	736
35	0.67	20.4	41	9.46	1660

best fit obtained, with the parameters shown in Tables I and II, respectively. One can observe that very good fits were obtained. The corresponding values of the energy dependence of the real and imaginary potentials for the ^{6}Li+^{116}Sn system are shown in Fig. 5. The analysis for the search of the TA or BTA in the scattering by the ^{112}Sn target was not possible, owing to the lack of more angular distribution data. These data will be used only in the next section to derive total reaction cross sections. The error bars in Fig. 5 represent the range of deviation of the potential corresponding to a χ^2 variation of one unit.

One can observe that the real and imaginary parts of the potential have roughly energy-independent behaviors at high energies. However, for this system, one can observe that the imaginary potential increases at the lowest energy below the barrier, and the real potential does not show any characteristic bell shape that corresponds to the usual TA. The present behavior corresponds to the presence of the BTA. This remark is based on the fact that the imaginary part of the optical potential does not drop to zero below the barrier energies, and also there is a decrease of the real potential at the lowest energies.

B. Analysis using the double-folding SPP

The SPP [52,53] is an optical potential that has been successfully used to describe a large variety of systems in a wide energy range, including fusion excitation functions

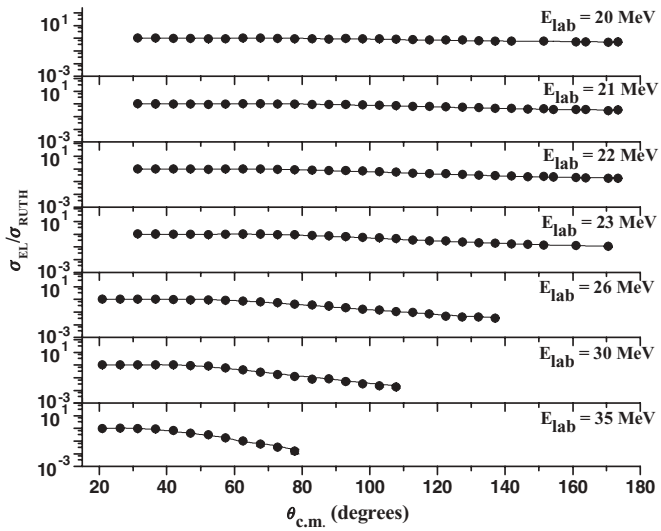

FIG. 3. Experimental elastic scattering cross sections normalized to the Rutherford cross sections for the ^{6}Li+^{116}Sn system and their best fits from optical model calculations. The curves corresponding to best fits were obtained using the Woods-Saxon potential (WSP).

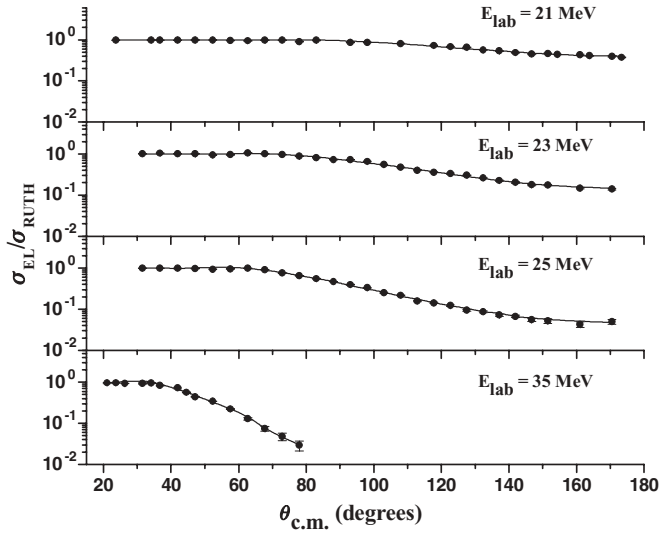

FIG. 4. Experimental elastic scattering cross sections normalized to the Rutherford cross sections for the ^{6}Li+^{112}Sn system and their best fits from optical model calculations. The curves corresponding to best fits were obtained using the Woods-Saxon potential (WSP).

and barrier distributions of weakly bound nuclei [55,56]. The trivial energy dependence of the bare interaction arises from the use of a local equivalent model based on the nonlocal nature of the interaction. At a limited range of energy, as occurs in the present work, it can be considered as the usual double-folding potential based on an extensive systematization of nuclear densities extracted from elastic scattering data. The imaginary part of the interaction is assumed to have the same shape as the real part, with one single adjustable parameter N_I related to its strength. The data-fit procedure is performed with only two free parameters, the normalization factors for the real and imaginary parts, N_R and N_I. The SPP has been used for the analysis of near barrier elastic scattering of weakly bound nuclei of several systems [19,29,30,35–40,42,51].

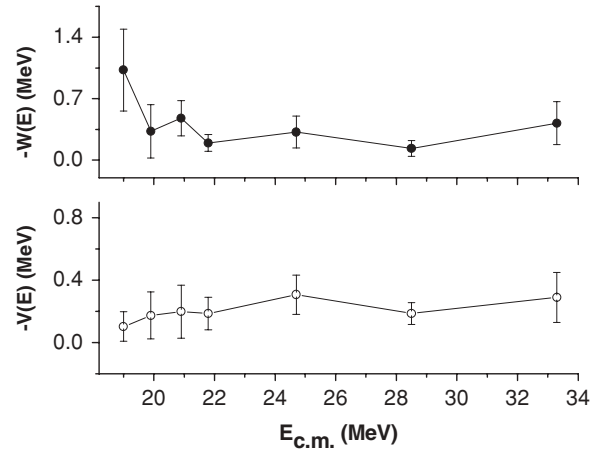

FIG. 5. Energy dependence of the real and imaginary parts of the optical potential obtained for the ^{6}Li+^{116}Sn system at an average radius $R_S = 9.40$ fm. The energy V_b of the Coulomb barrier is 22.07 MeV in the center-of-mass frame calculated using the Bass formula.

TABLE III. Parameters used with the SPP calculations for the ^{6}Li+^{116}Sn system.

$E_{\rm Lab}$ (MeV)	N_R	N_I	χ^2/n	σ_R (mb)
20	0.30	2.26	10.00	284
21	0.45	2.02	2.89	334
22	0.34	2.88	6.99	532
23	0.61	1.59	3.83	572
26	0.84	1.87	21.65	1071
30	0.83	0.95	10.44	1233
35	1.03	0.75	14.41	1599

The curves resulting from the best fits using the SPP hardly can be distinguished from those of the Woods-Saxon potential and therefore were not shown in Figs. 3 and 4. The resulting fits of the normalization parameters for the ^{6}Li+^{116,112}Sn system are shown in Tables III and IV. It can be observed that the energy dependence (Fig. 6) follows the same trend as in the previous analysis. So, our conclusions concerning the behavior of the OP energy dependence do not change when either potential is used.

IV. TOTAL REACTION CROSS SECTIONS FOR DIFFERENT SYSTEMS

If one wants to perform a systematic study of excitation functions for different systems, it is required to suppress differences arising from the size and charges of the systems. Nowadays the widely used "reduction" method was proposed by Gomes *et al.* [57]. In this method, the quantities $\sigma_R/(A_P^{1/3}+A_T^{1/3})^2$ vs $E_{\rm c.m.}(A_P^{1/3}+A_T^{1/3})^2/Z_P Z_T$ are plotted, where P and T are related to the projectile and target, respectively, and σ_R is the total reaction cross section. The authors claim that this procedure removes the dependence on the masses and charges of the collision partners but not specific features of the projectile density, particularly important when weakly bound projectile nuclei are involved. However, recently a new "reduction method" to compare fusion cross sections of different systems was proposed [26,27], later extended to be used with total reaction cross sections [58]. The new prescription is to plot the dimensionless quantities $F_R(x) = (2E_{\rm c.m.}/\hbar\omega R_B^2)\sigma_R$ vs $x = (E_{\rm c.m.} - V_B)/\hbar\omega$. Here, V_B, R_B, and $\hbar\omega$ are the height, radius, and curvature parameter of the Coulomb barrier, respectively, and $F_R(x)$ is called the total reaction function. Some reported works follow this new procedure [59–62].

TABLE IV. Parameters used with the SPP calculations for the ^{6}Li+^{112}Sn system.

$E_{\rm Lab}$ (MeV)	N_R	N_I	χ^2/n	σ_R (mb)
21	0.79	2.08	4.21	250
23	0.85	2.01	4.85	496
25	1.01	1.80	6.12	733
35	1.23	3.16	9.00	1691

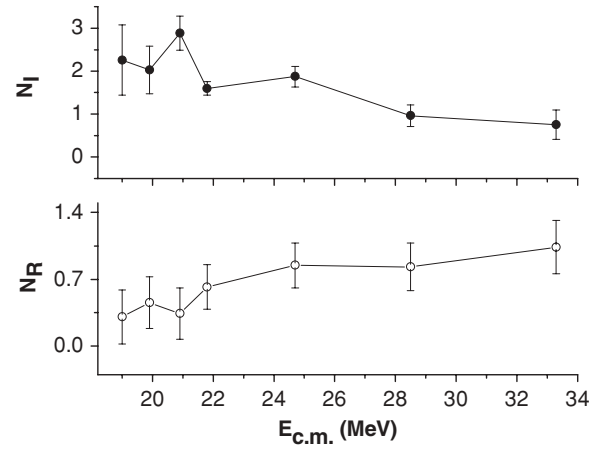

FIG. 6. Best fits for N_R and N_I as a function of the bombarding energy obtained from fits with the SPP for the ^{6}Li+^{116}Sn system. The energy V_b of the Coulomb barrier is 22.07 MeV in the center-of-mass frame calculated using the Bass formula.

In the present work we compare the total reaction cross sections derived from our experimental elastic scattering data for the ^{6}Li+^{116,112}Sn systems with other systems involving tightly bound, stable weakly bound, and radioactive and halo projectiles with targets in the same mass range. We use both mentioned procedures. Tables I–IV show the derived total reaction cross sections for the two systems measured in the present work.

Figure 7 shows the reduced total reaction cross sections for several systems, by using the reduction prescription of Gomes *et al.* [57], whereas Fig. 8 shows the total reaction functions for the same systems, plotted as proposed by Shorto *et al.* [58]. The systems analyzed are as follows: ^{6}Li+^{112,116}Sn (present

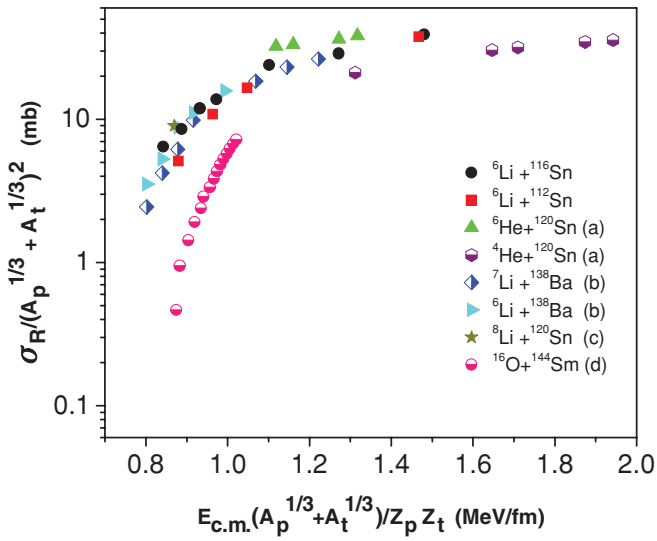

FIG. 7. (Color online) Reduced reaction cross section vs reduced projectile energy for the ^{6}Li+^{116,112}Sn reactions using the prescription given in Ref. [57], compared to other systems of similar masses: (a) From Ref. [59], (b) from Ref. [18], (c) from Ref. [60], and (d) from Ref. [63]. The reaction cross sections were obtained from optical model fits of the experimental angular distributions.

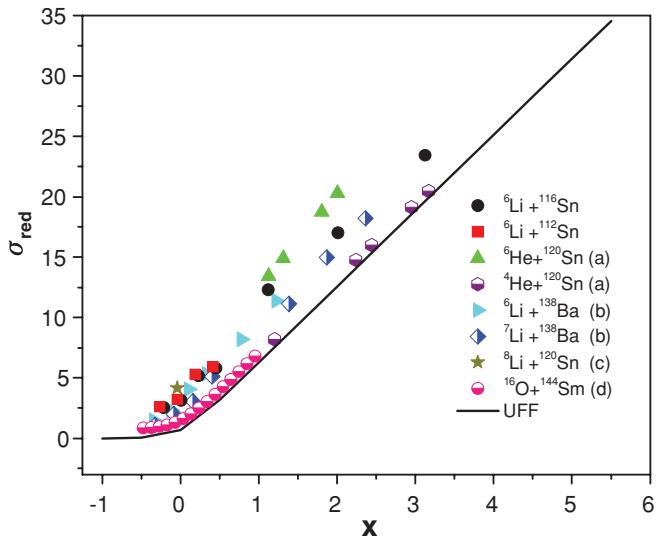

FIG. 8. (Color online) Reduced reaction cross section vs reduced projectile energy for the ^{6}Li+^{116,112}Sn reactions using the prescription given in Ref. [58], compared to other systems of similar masses: (a) From Ref. [59], (b) from Ref. [18], (c) from Ref. [60], and (d) from Ref. [63]. The reaction cross sections were obtained from optical model fits of the experimental angular distributions.

work), ^{4,6}He+^{120}Sn [59], ^{8}Li+^{120}Sn [60], ^{6,7}Li+^{138}Ba [18], ^{6,7}Li+^{144}Sm [41], ^{9}Be+^{144}Sm [38], and ^{16}O+^{144}Sm [63]. The systems with the targets ^{120}Sn and ^{138}Ba have been analyzed already in Ref. [59].

From Fig. 7 we observe that the total reaction cross section is largest for the neutron-halo ^{6}He projectile, which has a very low breakup energy (0.98 MeV). Then there is the group of lithium isotope projectiles (^{6,7,8}Li), with a breakup threshold between 1.5 and 2.5 MeV. Finally, the tightly bound projectiles ^{16}O and ^{4}He produce total reaction cross sections smaller than the weakly bound projectiles. So we conclude that the breakup increases the total reaction cross section, and for the ^{6}He nucleus, with a larger breakup probability than the lithium isotopes, the cross section is even larger. This is not the same conclusion obtained for a similar analysis with the light ^{27}Al target, for which it was found [64] that reaction cross sections induced by ^{6}He are similar to the ones induced by stable weakly bound projectiles. However, for light systems, the Coulomb breakup should be much smaller than for the systems analyzed in the present work. Moreover, the transfer channels may have a different influence in different mass regions. From Fig. 8, using an alternative reduction method, one can observe that the same conclusions can be drawn.

V. SUMMARY AND CONCLUSIONS

We have measured precise elastic scattering angular distributions, at near barrier energies, for the weakly bound ^{6}Li+^{116,112}Sn systems. The optical model analyses of the energy dependence of the interaction potential, performed by two different kinds of potentials, show the absence of the usual TA, corresponding to the presence of the so-called BTA. This behavior is attributed to the repulsive polarization potential produced by the breakup process. The analysis of total reaction cross sections for several systems with similar target masses indicates that the breakup increases the total reaction cross section in such a way that the neutron-halo ^{6}He projectile-induced reactions have larger cross sections than the not so weakly bound lithium isotopes, which, however, have larger cross sections than the tightly bound projectiles investigated.

ACKNOWLEDGMENTS

The authors wish to thank the operating staff of the BARC-TIFR Pelletron, Mumbai, India for the smooth running of the accelerator during the experiment. One of the authors (S.M.) thanks the DAE-BRNS, Mumbai for financial support through a major research project. S.M. also thanks UNESCO-TWAS and Conselho Nacional de Desenvolvimento Cientifico e Tecnológico (CNPq) for financial support during a visit to Brazil for this work. J.L. and P.R.S.G. thank the Conselho Nacional de Desenvolvimento Cientifico e Tecnológico (CNPq) and Fundação de Amparo a Pesquisa o Estado do Rio de Janeiro (FAPERJ) for partial financial support.

[1] M. A. Nagarajan, C. C. Mahaux, and G. R. Satchler, Phys. Rev. Lett. **54**, 1136 (1985).
[2] G. R. Satchler, Phys. Rep. **199**, 147 (1991).
[3] M. E. Brandan and G. R. Satchler, Phys. Rep. **285**, 143 (1997).
[4] C. Mahaux, H. Ngo, and G. R. Satchler, Nucl. Phys. A **449**, 354 (1986).
[5] G. R. Satchler and W. Love, Phys. Rep. **55**, 183 (1979).
[6] L. F. Canto, P. R. S. Gomes, R. Donangelo, and M. S. Hussein, Phys. Rep. **424**, 1 (2006).
[7] D. J. Hinde, M. Dasgupta, B. R. Fulton, C. R. Morton, R. J. Wooliscroft, A. C. Berriman, and K. Hagino, Phys. Rev. Lett. **89**, 272701 (2002).
[8] E. F. Aguilera *et al.*, Phys. Rev. Lett. **84**, 5058 (2000).
[9] E. F. Aguilera *et al.*, Phys. Rev. C **63**, 061603(R) (2001).
[10] C. Signorini, Eur. Phys. J. A **13**, 129 (2002).
[11] C. Signorini *et al.*, Phys. Rev. C **67**, 044607 (2003).
[12] Y. W. Wu *et al.*, Phys. Rev. C **68**, 044605 (2003).
[13] A. Pakou *et al.*, Phys. Lett. B **556**, 21 (2003).
[14] A. Pakou *et al.*, Phys. Rev. C **69**, 054602 (2004).
[15] A. Pakou, Phys. Rev. C **78**, 067601 (2008).
[16] P. R. S. Gomes *et al.*, Phys. Lett. B **634**, 356 (2006).
[17] N. Keeley *et al.*, Nucl. Phys. A **571**, 326 (1994).
[18] A. M. M. Maciel *et al.*, Phys. Rev. C **59**, 2103 (1999).
[19] J. Lubian *et al.*, Nucl. Phys. A **791**, 24 (2007).
[20] J. Lubian, T. Correa, P. R. S. Gomes, and L. F. Canto, Phys. Rev. C **78**, 064615 (2008).

[21] J. Lubian, T. Correa, E. F. Aguilera, L. F. Canto, A. Gomez-Camacho, E. M. Quiroz, and P. R. S. Gomes, Phys. Rev. C **79**, 064605 (2009)
[22] Y. Sakuragi, M. Yahiro, and M. Kamimura, Prog. Theor. Phys. **70**, 1047 (1983).
[23] N. Keeley and K. Rusek, Phys. Lett. B **427**, 1 (1998).
[24] N. Keeley, K. W. Kemper, and K. Rusek, Phys. Rev. C **66**, 044605 (2002).
[25] V. N. Garcia, J. Lubian, P. R. S. Gomes, A. Gomez-Camacho, and L. F. Canto, Phys. Rev. C **80**, 037602 (2009).
[26] L. F. Canto *et al.*, J. Phys. G **36**, 015109 (2009).
[27] L. F. Canto *et al.*, Nucl. Phys. A **821**, 51 (2009).
[28] P. R. S. Gomes, J. Lubian, and L.F. Canto, Phys. Rev. C **79**, 027606 (2009).
[29] M. S. Hussein, P. R. S. Gomes, J. Lubian, and L. C. Chamon, Phys. Rev. C **73**, 044610 (2006).
[30] P. R. S. Gomes *et al.*, J. Phys. (London) G **31**, S1669 (2005).
[31] S. B. Moraes *et al.*, Phys. Rev. C **61**, 064608 (2000).
[32] J. Lubian *et al.*, Phys. Rev. C **64**, 027601 (2001).
[33] R. J. Woolliscroft, B. R. Fulton, R. L. Cowin, M. Dasgupta, D. J. Hinde, C. R. Morton, and A. C. Berriman, Phys. Rev. C **69**, 044612 (2004).
[34] I. Martel *et al.*, Nucl. Phys. A **605**, 417 (1996).
[35] P. R. S. Gomes *et al.*, Phys. Rev. C **70**, 054605 (2004).
[36] P. R. S. Gomes *et al.*, Phys. Rev. C **71**, 034608 (2005).
[37] P. R. S. Gomes *et al.*, Phys. Rev. C **73**, 064606 (2006).
[38] P. R. S. Gomes *et al.*, Nucl. Phys. A **828**, 233 (2009).
[39] J. M. Figueira *et al.*, Phys. Rev. C **73**, 054603 (2006).
[40] J. M. Figueira *et al.*, Phys. Rev. C **75**, 017602 (2007).
[41] J. M. Figueira *et al.*, Phys. Rev. C **81**, 024613 (2010).
[42] J. O. Fernandez Niello *et al.*, Nucl. Phys. A **787**, 484c (2007).
[43] A. Gómez Camacho, P. R. S. Gomes, J. Lubian, E. F. Aguilera, and I. Padrón, Phys. Rev. C **76**, 044609 (2007).
[44] A. Gómez Camacho, P. R. S. Gomes, J. Lubian, and I. Padrón, Phys. Rev. C **77**, 054606 (2008).
[45] H. Kumawat *et al.*, Phys. Rev. C **78**, 044617 (2008).
[46] C. Signorini *et al.*, Phys. Rev. C **61**, 061603(R) (2000).
[47] M. Zadro *et al.*, Phys. Rev. C **80**, 064610 (2009).
[48] M. Biswas *et al.*, Nucl. Phys. A **802**, 67 (2008).
[49] E. F. Aguilera *et al.*, Phys. Rev. C **79**, 021601(R) (2009).
[50] A. R. Garcia *et al.*, Phys. Rev. C **76**, 067603 (2007).
[51] A. Gómez Camacho *et al.*, Nucl. Phys. A **833**, 156 (2010).
[52] L. C. Chamon, D. Pereira, M. S. Hussein, M. A. Cândido Ribeiro, and D. Galetti, Phys. Rev. Lett. **79**, 5218 (1997).
[53] L. C. Chamon *et al.*, Phys. Rev. C **66**, 014610 (2002).
[54] J. Raynal, Phys. Rev. C **23**, 2571 (1981).
[55] E. Crema, L. C. Chamon, and P. R. S. Gomes, Phys. Rev. C **72**, 034610 (2005).
[56] E. Crema, P. R. S. Gomes, and L. C. Chamon, Phys. Rev. C **75**, 037601 (2007).
[57] P. R. S. Gomes, J. Lubian, I. Padron, and R. M. Anjos, Phys. Rev. C **71**, 017601 (2005).
[58] J. M. B. Shorto *et al.*, Phys. Lett. B **678**, 77 (2009).
[59] P. N. de Faria *et al.*, Phys. Rev. C **81**, 044605 (2010).
[60] P. N. de Faria, Ph.D. thesis, IFUSP, 2009.
[61] S. Mukherjee *et al.*, Eur. Phys. J. A **45**, 23 (2010).
[62] A. Lemasson *et al.*, Phys. Rev. Lett. **103**, 232701 (2009).
[63] J. R. Leigh *et al.*, Phys. Rev. C **52**, 3151 (1995).
[64] E. A. Benjamim *et al.*, Phys. Lett. B **647**, 30 (2007).